HOKKAIDO UNIVERSITY

Title	Non-destructive evaluation of the strain distribution in selected-area He+ ion irradiated 4H-SiC
Author(s)	Yang, Subing; Tokunaga, Sakiko; Kondo, Minako et al.
Citation	Applied surface science, 500, 144051 https://doi.org/10.1016/j.apsusc.2019.144051
Issue Date	2020-01-15
Doc URL	https://hdl.handle.net/2115/83831
Rights	© 2020. This manuscript version is made available under the CC-BY-NC-ND 4.0 license http://creativecommons.org/licenses/by-nc-nd/4.0/
Rights(URL)	https://creativecommons.org/licenses/by-nc-nd/4.0/
Type	journal article
File Information	revised Manuscript.pdf

Non-destructive evaluation of the strain distribution in selected-area He^{+} ion irradiated 4H-SiC

Subing Yang [a], Sakiko Tokunaga [a], Minako Kondo [b], Yuki Nakagawa [b], Tamaki Shibayama [b, *]

a Graduate School of Engineering, Hokkaido University, Sapporo, Hokkaido 060-8628, Japan

b Faculty of Engineering, Hokkaido University, Sapporo, Hokkaido 060-8628, Japan

* Corresponding author.

E-mail address: shiba@qe.eng.hokudai.ac.jp

Residual strain in silicon carbide (SiC) greatly affects its physical and chemical properties and thus the performance of SiC-based devices. Herein, the detailed strain distribution in selected-area He^{+} ion-irradiated 4H-SiC was evaluated using the non-destructive techniques of electron backscattering diffraction and confocal Raman microscopy (CRM). In addition to the strain introduced in the irradiated area, excessive strain induced by irradiation-induced swelling also extended into the surrounding substrate. Furthermore, great compressive strain was concentrated around the interface between the irradiated and unirradiated areas. In the strain-introduced substrate, an $A_1(LO)/A_1(LOPC)$ peak variation was detected by CRM, suggesting a variation of the carrier density.

1. Introduction

Silicon carbide (SiC) has drawn great attention for electronic and optical applications, and especially in severe environments such as high temperature, high voltage and irradiation fields, owing to its excellent mechanical, optical and electronic properties [1-3]. For high-performance SiC-based electronic devices, ion implantation is widely used for selected-area doping because of the low diffusivity of dopant impurities in SiC [2]. However, high residual strain is introduced into the SiC devices via irradiation-induced damage [4-6], which greatly influences the mechanical, electronic [7] and optical properties of SiC [8]. Furthermore, large residual stress can induce cracking and thus increases the risk of device failure [9,10]. Therefore, evaluation of the residual strain state in SiC devices has become very important for their fabrication and application.

In the past two decades, irradiation-induced residual strain in SiC has been widely investigated by X-ray diffraction (XRD) [4,11-14], providing important insights into strain formation and accumulation under different irradiation conditions. However, most of these strain evaluations have been performed in homogeneously-irradiated materials or in the homogeneous region of a selected-area ion-implanted sample. Few detailed strain distribution studies in the selected-area ion-implanted SiC devices have been reported owing to the relatively low spatial resolution of XRD. For the development of advanced SiC-based devices, a full understanding of the strain distribution in the whole selected-area ion-implanted SiC is necessary, which needs a technique with a high spatial and strain resolution.

2

Recently, electron backscattered diffraction (EBSD) has become an increasingly important non-destructive technique for measuring the residual strain on the surface of crystalline materials with high spatial resolution (<50 nm) [15, 16]. Using cross-correlation analysis of the EBSD pattern, strain sensitivity on the level of about 10^{-4} has already been obtained [17]. In the past decade, the EBSD technique has been used to measure the strain in various semiconductors [15, 18,19]. However, few studies of selected-area ion-implanted SiC devices have been reported. Owing to its clear advantages of non-destructive measurements, ease in sample preparation and high sensitivity, Raman scattering has become a powerful technique for characterization of semiconductors [4,20]. Based on the confocal Raman microscopy (CRM) technique, the stress distribution in Si around the indentation has been revealed at the sub-micrometer scale [19]. The CRM technique may also be appropriate to evaluate the detailed strain distribution in selected-area ion-implanted SiC.

To investigate the strain distribution in the whole selected-area ion-implanted SiC, these two promising techniques of EBSD and CRM were used to evaluate selected-area He$^+$ ion-irradiated 4H-SiC. A detailed normal strain distribution in the ion-irradiated 4H-SiC was first provided via comparison of the results of EBSD and CRM.

2. Experimental procedure

Herein, an n-type 4H-SiC (0001) single-crystal substrate (Xiamen Powerway Advanced Material Co., Ltd, Xiamen, China) about $10 \times 10 \times 0.33$ mm^3 was used. This substrate was irradiated with 100 keV He$^+$ ions at a fluence of up

to 5.09×10^{16} He·cm^{-2} at room temperature. To clearly distinguish between the irradiated and unirradiated areas, part of the sample was covered during irradiation by a mask with a hole 8 mm in diameter as shown in Fig. S1(a).

After irradiation, swelling of the irradiated area was measured using atomic force microscopy (AFM; KEYENCE VN–8000) by comparing the height difference between the irradiated and unirradiated areas. A field emission scanning electron microscope (SEM; JEOL JSM–7001FA) equipped with an EBSD detector was used, operating at an acceleration voltage of 20 kV, a sample tilt of 70° and a scan size and scan step of 20×20 μm^2 and 0.1 μm, respectively. EBSD patterns were stored as uncompressed, 12-bit gray scale in TIFF format and 1392×1040 pixels. To clearly describe the strain distribution, two orthogonal scanning regions were selected, and each contains both an irradiated and an unirradiated area. In one scanning region the X axis is vertical to the irradiated/unirradiated interface, and in the other Y axis is vertical to the interface. The detailed configuration of EBSD scanning was described in Fig. S1(b) of supplementary materials. The strain was obtained by analyzing the EBSD patterns using the CrossCourt 3 software. Regions of interest (ROIs) 256×256 pixels were described, and 20 ROIs were automatically selected. Comparing with SEM image, the irradiated/unirradiated interface location in the EBSD strain image was determined.

Beside the EBSD scanning regions, the Raman backscattering experiment was conducted at room temperature in Raman microscope (HORIBA XploRA) using a laser wavelength of 532 nm, where a 2400 groove/nm

grating and 100–2000 cm^{-1} scanning range were selected. The laser was focused to a spot ~2 μm in diameter. The Raman spectra data were collected using the CRM technique with a confocal aperture of 100 μm. The detection was carried out by the point-to-point method along a direction from the irradiated area to the unirradiated area. The peak positions were obtained by fitting the peak with a Voigt function (i.e., a weighted sum of a Gaussian and Lorentzian distribution) [4].

3. Results and discussion

3.1 Strain distribution evaluated by EBSD

After irradiation, swelling of the SiC was confirmed by AFM, where the surface of the irradiated area was 25.7 ±4.5 nm higher than that of substrate (shown in Fig. S2). Figure 1 shows the residual elastic strain maps measured by EBSD where the residual strain in the irradiated area exhibits an anisotropic distribution of positive and negative classification along the different directions. The positive classification of ε_{zz} indicates an expansion of the lattice spacing and tensile strain, which is in agreement with the swelling measured by AFM. In contrast, the ε_{xx} and ε_{yy} components exhibit compressive strain. In homogeneously-irradiated SiC, tensile strain is typically caused by a positive volume change of the crystal via the distortion field of the defects [4]. However, for selected-area ion-implanted SiC, the volume expansion is confined to the horizontal (*X*) and vertical (*Y*) directions in the irradiated area, which causes compressive strain in the *X* and *Y* directions and tensile strain in the *Z* direction.

Further, the strain distribution is also heterogeneous around the

irradiated/unirradiated interface, and a strain concentration is observed in this region. It is interesting to note that the strain-concentrated region for the ε_{xx} component covers both the irradiated and unirradiated areas. However, the concentration of the component ε_{yy} and ε_{zz} typically only appear in the irradiated area. In addition, the distribution of ε_{xx} indicates that strain is introduced not only into the irradiated area but also into the surrounding substrate, which should be attributed to the swelling of the irradiated area.

Fig.1.

3.2 Raman spectra variation

The microstructural variation and strain in the ion-irradiated SiC were next measured by CRM. The 4H-SiC exhibits Raman active modes of A_1, E_1 and E_2, where the A_1 and E_1 modes are split into longitudinal (LO) and transverse (TO) optical modes [20, 21]. To clearly clarify the variation of Raman spectrum, the spectra excited from three different positions, that is unirradiated area (P1), unirradiated region close to the interface (P2), and irradiated area (P3), are displayed in Fig. 2(a) (the schematic image of P1, P2 and P3 position is shown in Fig. S1(c) of supplementary materials). For the Raman spectrum excited from the unirradiated area (P1), the major peaks attributed to the Si–C vibration are labelled. The sharp peaks detected at 775.5 and 796.4 cm^{-1} correspond to the $E_2(TO)$ and $E_1(TO)$ modes [21]. The broad peak located around 982 cm^{-1} is attributed to A_1(longitudinal optical phonon–plasmon coupled (LOPC)) modes [18,20], whose line shape strongly depends on the carrier density [22,23]. The broad and weak peak of the $A_1(LOPC)$ peak herein implies a relatively high carrier density in our

sample. The peaks located at 200, 263 and 609 cm^{-1} are ascribed to the E$_2$(transverse acoustic (TA)), E$_1$(TA) and A$_1$(longitudinal acoustic (LA)) modes, which are the second-order Raman peaks of 4H-SiC [20, 21].

After He$^+$ ion irradiation, the Raman peaks of the crystal Si–C vibrations discussed above nearly disappear, and some new broad peaks appear (P3 in Fig. 2(a)). These new peaks are attributed to the vibration of the Si–Si bands (100–600 cm^{-1}), Si–C bands (700–1000 cm^{-1}) and C–C bands (1100–1800 cm^{-1}) [21]. The relative high intensity of the Si–Si and C–C vibrations indicate a high degree of disorder, even for an amorphous state, of SiC in the irradiated area [21]. The remaining E$_2$(TA) and E$_2$(TO) peaks imply that some short-range order is still maintained in the irradiated area. For the P2 position, located in the unirradiated area but close to the interface, the Raman spectra is similar to that of P1, suggesting a good crystallinity in this region. However, a sharp new peak identified as A$_1$(LO) [20] appears at 963 cm^{-1} beside the broad peak A$_1$(LOPC), suggesting a variation of carrier density and microstructure in this region that will be discussed later.

In addition to the above Raman mode variations, shifts in the peak positions for some Raman modes, such as the A$_1$(LA) and E$_2$(TO) modes, can be used for strain evaluation [20, 24]. Herein, the E$_2$(TO) mode was chosen to evaluate the strain because of its relatively high intensity, and its peak position at different surface locations is shown in Fig. 2. We assume that the effect of ion implantation is negligible at a distance of about 75 μm in the unirradiated area, and the spectrum at this location was regarded as a reference for the strain-free state. As shown in Figs. 2(b) and 2(c), the peak

position of the E_2(TO) mode at the strain-free state is about 774.4 cm^{-1} (measured by peak fitting with Voigt functions). With respect to the strain-free state reference spectrum, the E_2(TO) mode shifts to lower frequencies in the irradiated area and to higher frequencies in the unirradiated area close to the interface, corresponding to tensile and compressive strain states [20, 24, 25], respectively. Further, compressive strain was introduced into the surrounding substrate. The peak shift of E_2(TO) depends on the distance from the interface, indicating an inhomogeneous strain distribution in this region (Fig.2(d)). The largest peak shift is exhibited at the interface, signifying a strain concentration at this position that is consistent with the EBSD results. In addition, owing to strain or defects, the full width at half maximum of E_2(TO) also increases with proximity to the interface, which is shown in Fig. S3.

Fig. 2.

3.3 Comparison of strain distribution evaluated by EBSD and CRM

The quantitative results of the strain distribution measured by both EBSD and CRM are shown in Fig. 3. In EBSD, the statistical result was obtained by averaging the measured strain values obtained from a narrow surface area (i.e., column) parallel to the interface. For Raman measurements, Rohmfeld et al. have reported the relationship of the TO mode shift with the strain in 3C-SiC [25], which we have assumed to also be approximate for the 4H-SiC herein.

As shown in Fig. 3 (a), the EBSD results exhibit a strain distribution along three orientations. Near the left boundary of the EBSD scanning area, the

strain is relatively homogeneous, which may represent the strain state in the center of the irradiated area with an average of −0.00075, −0.00099 and +0.00036 in X, Y and Z directions, respectively. Moving toward the interface, strain concentration is clearly shown near the interface with a value of -0.0011, -0.0013 and +0.00043 for ε_{xx}, ε_{yy} and ε_{zz}, respectively.

As mentioned above that strain concentration region is different for ε_{xx}, ε_{yy}, which is more clearly shown in Fig. 3(a). Furthermore, it is interesting to note that virtually only the ε_{xx} strain extended into the unirradiated area, while the ε_{yy} and ε_{zz} strain sharply decreased and almost disappeared in the unirradiated area. Herein, the X, Y and Z directions correspond to the $[\bar{1}2\bar{1}0]$, $[10\bar{1}0]$ and $[0001]$ directions, respectively. To clarify the correlation between the strain distribution and the crystallographic orientation around the interface, the strain distribution in another region where the interface is vertical to the Y axis was measured, and the statistic results are shown in Fig. 3(b). Near the left boundary, the strain distribution shown in Fig. 3(b) is similar to that in Fig. 3(a). However, around the interface it is ε_{yy} rather than ε_{xx} that concentrated around the interface and dominantly extended into the unirradiated, when the interface is vertical to the Y axis. This suggests that around the interface, the distribution of ε_{xx} and ε_{yy} might be not attributed to the crystallographic orientation but to the correlation between strain direction and interface direction, and that strain may easier extend into the unirradiated area along the direction vertical to the interface. However, the strain along $[10\bar{1}0]$ (ε_{yy}) is always higher than that along $[\bar{1}2\bar{1}0]$ (ε_{xx}) in the Figs. 3(a) and 3(b), suggesting that the strain value of ε_{xx} and ε_{yy} may

9

correlate with the orientation. Besides, it is interesting to note that at the irradiated region about 2 μm to the interface where the ε_{zz} reaches a peak value, the distributions of ε_{xx} and ε_{yy} show a peak and a trough simultaneously in Fig. 3(a) (trough and peak for ε_{xx} and ε_{yy} in Fig. 3(b)), indicating an inverse variation of decrease and increase for ε_{xx} and ε_{yy} at this region. Irradiation induced defects result in different effects on the strain accumulation. For example, interstitials usually cause the volume expansion while vacancies cause the compressive strain. It has been reported that the interstitial configuration in 4H-SiC under ion irradiation is anisotropic [26]. Therefore, the relative degree of ε_{xx}, ε_{yy} and ε_{zz} and their simultaneous variation near the interface should be attributed to the configuration of defects for different crystallographic orientation.

In Figs. 3(c) and 3(d), the Raman measurement results indicate a relatively homogeneous tensile strain in the irradiated area. In the unirradiated area, a highest compressive strain is shown at the interface that gradually decreased with distance from the interface. The strain distribution evaluated by CRM exhibits good agreement with some EBSD results. For example, in the irradiated area, the tensile strain measured by CRM is consistent with the ε_{zz} strain in the EBSD results. Also, the strain distribution trend in the unirradiated area measured by CRM is also in good agreement with that of the EBSD results. Both EBSD and CRM are powerful techniques for high-spatial-resolution strain distribution evaluation of SiC. However, the EBSD results provide more information than CRM for the ion-irradiation-induced strain. For example, EBSD directly provides a correlation between the strain

and the orientation under irradiation condition. To determine the components of the strain along different directions using CRM, however, it may be necessary to implement off-axis and polarized excitation [27].

Fig. 3.

Although the EBSD is more convenient to explore the correlation between the strain and the orientation, CRM spectra can provide more information about variations in microstructure and electronic properties. For example, emergence of the $A_1(LO)$ peak and its variation in the unirradiated area close to the interface were observed by CRM (Fig. 4). Moving away from the interface into the unirradiated area, the $A_1(LO)$ peak gradually decreases in intensity (Fig. 4(b)) and shifts to higher frequencies (Fig. 4(c)), which suggests a gradual increasing of carrier density in this region and a coupling of the $A_1(LO)$ phonon to the plasmon mode (i.e., $A_1(LOPC)$ mode) [20, 23]. Further, both the A_1 (LO) peak position and intensity exhibits a dependence on the distance to the interface, and both exhibits a similar trend with the strain distribution estimated by CRM and EBSD in this region. This implies that the appearance and variation of the $A_1(LO)$ mode can be attributed to the effect that strain and defects have on the carrier density, which will be further studied by transmission electron microscopy equipped with an electron energy-loss spectrometer. Carrier density uniformity is important for the performance of 4H-SiC as a semiconductor. Thus, the strain/stress effect on the carrier density of SiC should be taken into consideration during fabrication and application.

4. Conclusions

In summary, detailed strain distributions in the selected-area He^+ ion-irradiated 4H-SiC was evaluated by EBSD and CRM, whose results show good agreement. Strain is shown to not only be introduced into the irradiated area, but also to extend into the unirradiated substrate owing to irradiation-induced swelling. Furthermore, a higher compressive strain is concentrated around the interface between the irradiated and unirradiated areas. The relative strain degree shows correlation with the crystallographic orientation, and the strain distribution around the interface may be determined by the correlation between the strain and interface direction. Variation of the $A_1(LO)$ mode peak was observed by CRM in the strain-introduced substrate, which may be attributed to the effect of strain and defects on the carrier density in this region.

for editing a draft of this manuscript.

References

[1] X. She, A. Q. Huang, O. Lucıa, B. Ozpineci, Review of silicon carbide power devices and their applications, IEEE Trans. Industr. Electron. 64 (2017) 8193.

[2] N. G. Wright, A. B. Horsfall, K. Vassilevski, Prospects for SiC electronics and sensors, Mater. Today 11 (2008) 16.

[3] S. Castelletto, B. C. Johnson, V. Ivády, N.Stavrias, T. Umeda, A. Gali, T. Ohshima, A silicon carbide room-temperature single-photon source, Nature Mater. 13 (2014) 151.

[4] X. Chen, W. Zhou, Q. Feng, J. Zheng, X. Liu, B. Tang, J. Li, J. Xue, S. Peng, Irradiation effects in 6H-SiC induced by neutron and heavy ions: Raman spectroscopy and high-resolution XRD analysis, J. Nucl. Mater. 478 (2016) 215.

[5] S. Sasaki, J. Suda, T. Kimoto, Lattice mismatch and crystallographic tilt induced by high-dose ion-implantation into 4H-SiC, J. Appl. Phys. 111 (2012) 103715.

[6] A. Ashraf Ali, J. Kumar, V. Ramakrishnan, K. Asokan, Raman spectroscopic study of He ion implanted 4H and 6H-SiC, Mater. Lett. 213 (2018) 208.

[7] A. Qamar, D. V. Dao, P. Tanner, H. Phan, T. Dinh, S. Dimitrijev, Influence of external mechanical stress on electrical properties of single-crystal n-3C-SiC/p-Si heterojunction diode, Appl. Phys. Expr. 8 (2015) 061302.

[8] K. Lee, Isnaeni, Y. Yoo, J. Lee, Y. Kim, Y. Cho, Influence of defect reduction and strain relaxation on carrier dynamics in InGaN-based light-emitting diodes on cone-shaped patterned sapphire substrates, J. Appl. Phys. 113 (2013) 173512.

[9] S. Tsukimoto, T. Ise, G. Maruyama, S. Hashimoto, T. Sakurada, J. Senzaki, T. Kato, K. Kojima, H. Okumura, Local strain distribution and microstructure of grinding-induced damage layers in SiC wafer, J. electron. Mater. 47 (2018) 6722.

[10] X. Xie, X. Hu, X. Chen, F. Liu, X. Yang, X. Xu, H. Wang, J. Li, P. Yu, R. Wang, Characterization of the three-dimensional residual stress distribution in SiC bulk crystals by neutron diffraction, CrystEngComm, 19 (2017) 6527.

[11] Y. Yang, J. Guo, B. Raghothamachar, X. Chan, T. Kim, M. Dudley, Characterization of strain due to nitrogen doping concentration variations in heavy doped 4H-SiC, J. Electronic Mater. 47 (2018) 938.

[12] A. Debelle, L. Thome, D. Dompoint, A. Boulle, F. Garrido, J. Jagielski, D. Chaussende, Characterization and modelling of the ion irradiation induced disorder in 6H-SiC and 3C-SiC single crystals, J. Phys. D: Appl. Phys. 43 (2010) 455408.

[13] S. Leclerc, A. Declémy, M. F. Beaufort, C. Tromas, J. F. Barbot, Swelling of SiC under helium implantation, J. Appl. Phys. 98 (2005) 113506.

[14] D.J. Sprouster, T. Koyanagib, E. Dooryheec, S. K. Ghose c, Y. Katohb, L. E. Ecke, Swelling of SiC under helium implantation, Scripta Mater. 143

(2018) 176.

[15] X. Li, Z. Lia, X. F. Tao, L. L. Ren, S. T. Gao, G. F. Xu, Distribution of residual strain around nanoindentations in silicon, Mater. Lett. 132 (2014) 285.

[16] S. I. Wright, M. M. Nowell, and D. P. Field. A review of strain analysis using electron backscatter diffraction, Microsc. Microanal. 17 (2011) 316.

[17] A. J. Wilkinson, T. B. Britton, J. Jiang and P. S. Karamched, A review of advances and challenges in EBSD strain mapping, IOP Conf. Ser.: Mater. Sci. Eng. 55 (2014) 012020.

[18] W. Osborn, L. H. Friedman, M. Vaudin, Strain measurement of 3D structured nanodevices by EBSD, Ultramicroscopy 184 (2018) 88.

[19] M. D. Vaudin, Y. B. Gerbig, S. J. Stranick, R. F. Cook, Comparison of nanoscale measurements of strain and stress using electron back scattered diffraction and confocal Raman microscopy, Appl. Phys. Lett. 93 (2008) 193116.

[20] S. Nakashima, H. Harima, Raman investigation of SiC polytypes, Phys. stat. sol. (a) 162 (1997) 39.

[21] S. Sorieul, J. M. Costantini, L. Gosmain, L. Thome, J. J. Grob, Raman spectroscopy study of heavy-ion-irradiated α-SiC, J. Phys.: Condens. Matter. 18 (2006) 5235.

[22] T. Koyanagi, M. J. Lance, Y. Katoh, Quantification of irradiation defects in beta-silicon carbide using Raman spectroscopy, Scripta Mater. 125 (2016) 58.

[23] S. Nakashima, T. Mitani, J. Senzaki, H. Okumura, T. Yamamoto, Deep

ultraviolet Raman scattering characterization of ion-implanted SiC crystals, J. Appl. Phys. 97 (2005) 123507.

[24] S. Nakashima, T. Kato, S. Nishizawa, T. Mitani, H. Okumura, T. Yamamotob, Deep ultraviolet Raman microspectroscopic characterization of polishing-induced surface damage in SiC crystals, J. Electrochem. Soc. 153 (2006) 319.

[25] S. Rohmfeld, M. Hundhausen, L. Ley, C.A. Zorman, M. Mehregany, Quantitative evaluation of biaxial strain in epitaxial 3C-SiC layers on Si (100) substrates by Raman spectroscopy, J. Appl. Phys. 91 (2002) 1113.

[26] Y. Zhang, F. Gao, W. Jiang, D. E. McCready, and W. J. Weber, Damage accumulation and defect relaxation in 4H-SiC, Phys. Rev. B 70(2004), 125203.

[27] G. H. Loechelt, N. G. Cave, J. Menendez, Polarized off-axis Raman spectroscopy: A technique for measuring stress tensors in semiconductors, J. Appl. Phys. 86 (1999) 6164.
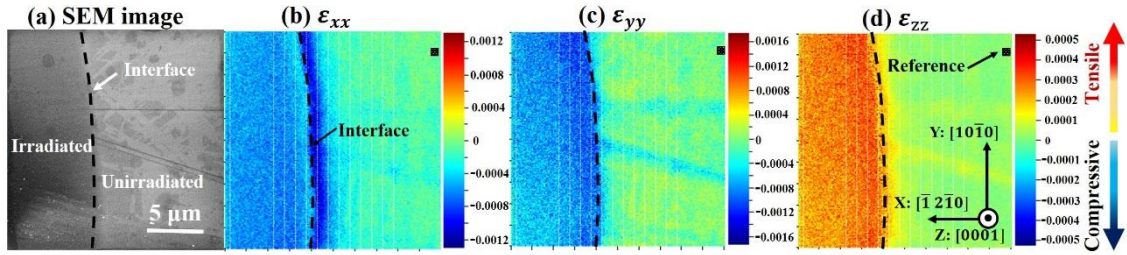
Fig. 1. Strain distribution around the irradiated/unirradiated interface. (a) SEM image, (b–d) residual elastic strains (b) ε_{xx}, (c) ε_{yy}, and (d) ε_{zz}, respectively representing the strain horizontal (X), vertical (Y) and normal to the sample surface (Z). The EBSD pattern obtained from the black dot (Reference) is regarded as the reference for the strain analysis. Strain detected at some positions where are not affected by irradiation is due to the scratch on the sample surface.
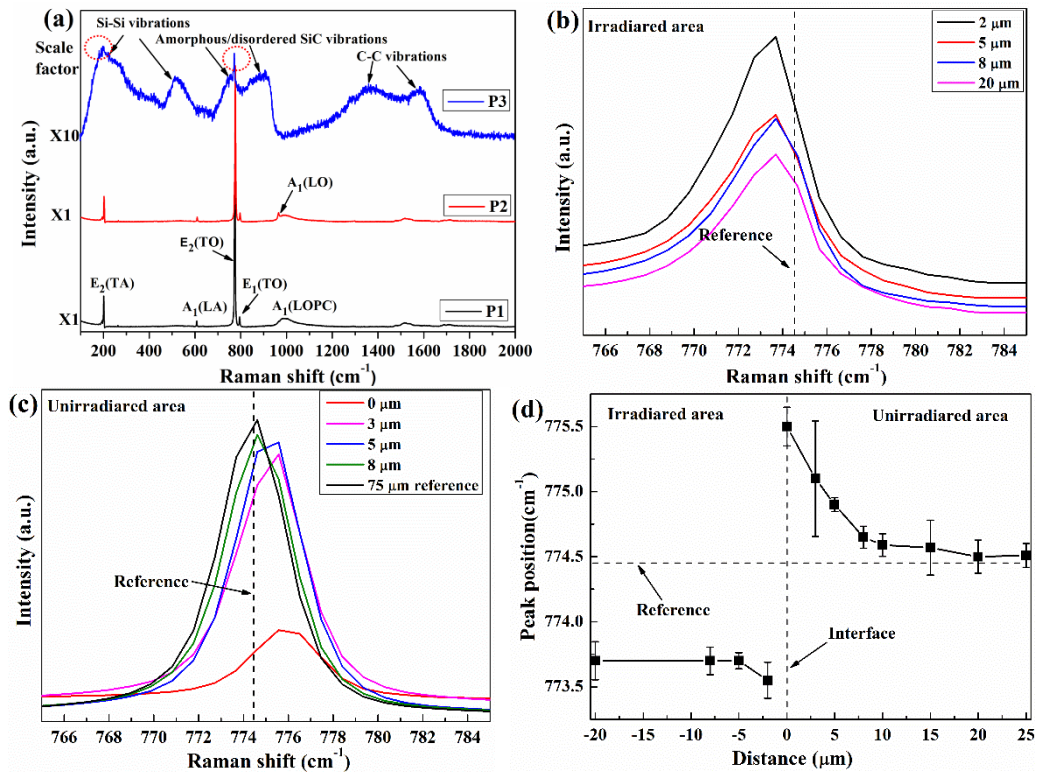
Fig. 2. Variation of Raman spectra from different locations in the 4H-SiC irradiated by He$^+$ ions. (a) Raman spectra from different location, representing the unirradiated region (P1), unirradiated region close to the interface (P2), and irradiated area (P3). (A schematic image of the P1, P2 and P3 locations is given in Fig. S1(c) in the Supplementary Materials. (b, c) Peak shift of E$_2$(TO) in the (b) irradiated and (c) unirradiated areas. The insert numbers represent the distance from the interface. (d) Peak position of E$_2$(TO) as a function of the distance to the interface.
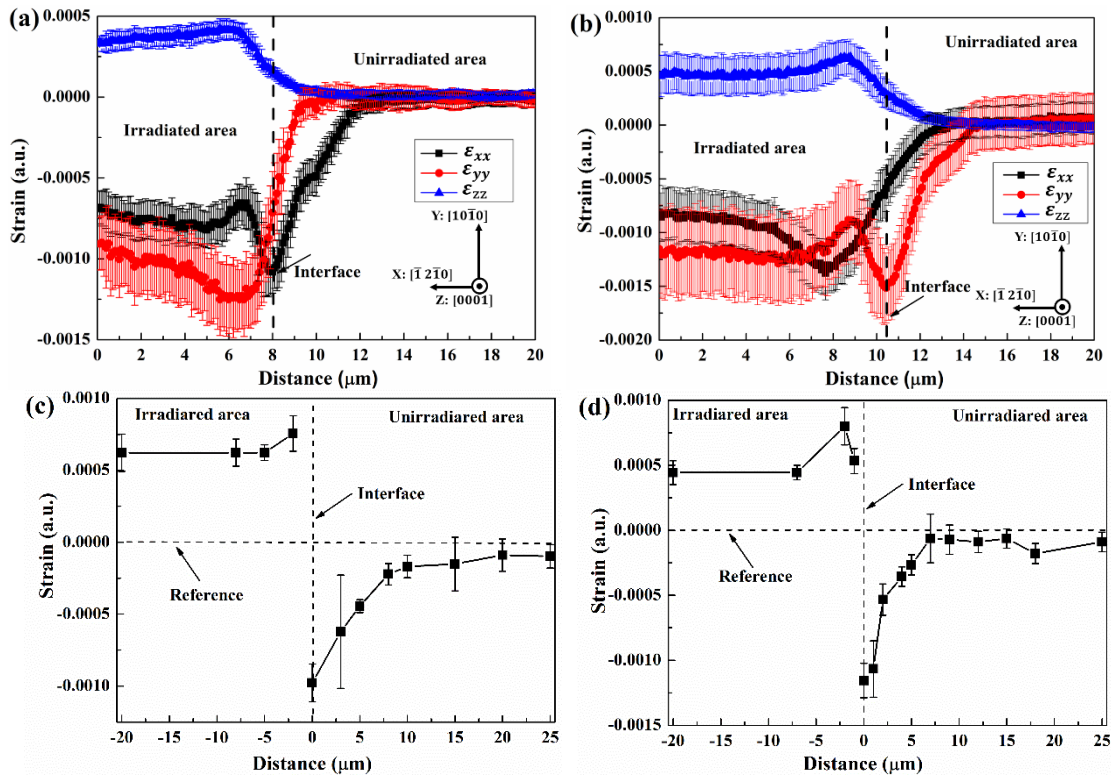
Fig. 3. Strain distribution measured by (a, b) EBSD and (c, d) CRM. (a) and (c) are acquired from the same region where the interface of unirradiated/irradiated area is vertical to the X axis, corresponding to the Fig. 1 and Fig. 2 for EBSD and CRM, respectively. (b) and (d) are acquired from another region where the interface of unirradiated/irradiated area is vertical to the Y axis, and their original EBSD scanning images and Raman spectra are shown in Fig. S4 and Fig. S5, respectively.
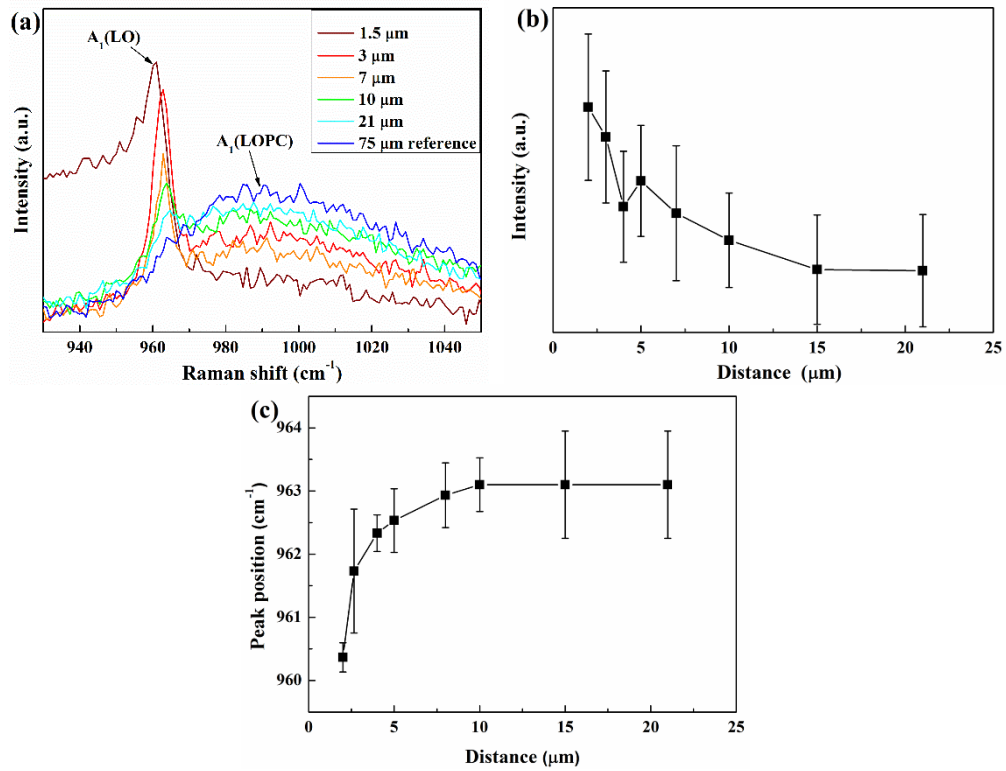
Fig. 4. Distribution of the $A_1(LO)$ mode in the unirradiated area close to the interface. (a) Variation of the $A_1(LO)$ peak (b) intensity and (c) peak position of $A_1(LO)$ as a function of the distance from the interface.

<p align="center">**Supplementary Materials**</p>

Non-destructive evaluation of the strain distribution in selected-area He⁺ ion irradiated 4H-SiC

Subing Yang [a], Sakiko Tokunaga [a], Minako Kondo [b], Yuki Nakagawa [b], Tamaki Shibayama [b, *]

a Graduate School of Engineering, Hokkaido University, Sapporo, Hokkaido 060-8628, Japan

b Faculty of Engineering, Hokkaido University, Sapporo, Hokkaido 060-8628, Japan

* Corresponding author.

E-mail address: shiba@qe.eng.hokudai.ac.jp

1. Experimental procedure

1.1 Irradiation procedure

During ion irradiation, a mask with a hole of 8 mm in diameter was used to cover the sample to distinguish the irradiated area and unirradiated area, as shown in Fig. S1(a).

1.2 EBSD scanning arrangement

Two scanning regions were selected as shown in Fig. S1(b). The scanned region contained both an irradiated and an unirradiated area. During EBSD scanning, the boundary between the irradiated and unirradiated areas was set almost vertical (region 1) or horizontal (region 2) to the scanning direction, which was convenient for the sequent statistics analysis whereby the strain values of each column were averaged.

1.2 CRM experiment

The detailed strain distribution evaluation was obtained by point-to-point measurements progressing from the irradiated area to the unirradiated area. A schematic image of the measurement procedure is shown in Fig. S1(c), illustrating Position 3 (P3) in the irradiated area, Position 2 (P2) in the unirradiated area close to the irradiated/unirradiated interface, and Position 1 (P1) in the unirradiated area relatively far from the interface.
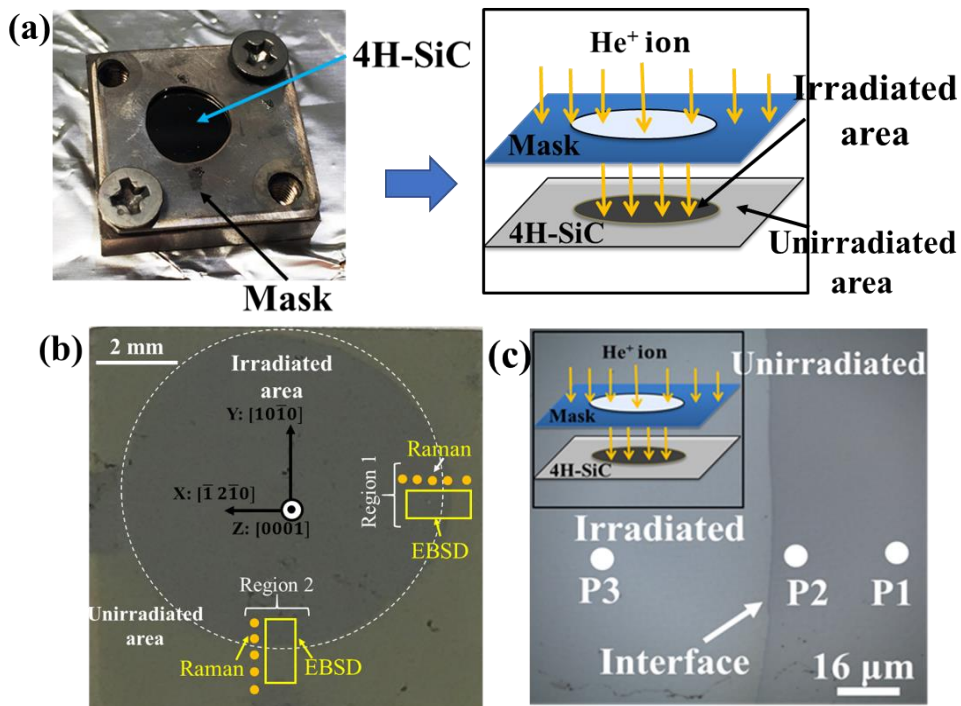
Fig. S1. Schematic images of experiment configuration. (a) Sample arrangement during ion implantation (b) EBSD and Raman scanning regions. (c) the P1, P2 and P3 locations mentioned in Fig. 2(a) of manuscript.

2. Atomic force microscopy results

Figure S2 was acquired as a screenshot from the atomic force microscope (AFM) instrument, showing the surface height distribution in the horizontal (Fig. S2(b)) and vertical (Fig. S2(c)) directions. The height difference between the irradiated area (left green dashed line in Fig. S2(b)) and the unirradiated area (right green dashed line in Fig. S2(b)) are enumerated as 27.9 nm in Fig. S2(d) (red circled data).
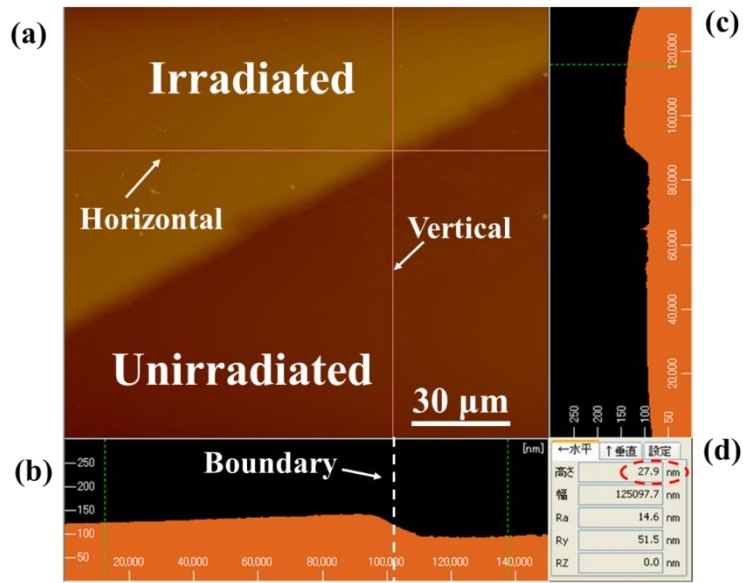
Fig. S2. AFM image of 4H-SiC surface. (a) AFM surface image. (b) Height distribution in horizontal direction. (c) Height distribution in vertical direction. (d) Height difference for the two positions pointed out in (b).

3. The full width at half maximum of E_2(TO)

The full width at half maximum (FWHM) of E_2(TO) peak was obtained by fitting the peak with a Voigt function. Owing to strain or defects, the FWHM of E_2(TO) increases with proximity to the interface. In the irradiated area, however, the FWHM of E_2(TO) is difficult to measure because of the high background signal.
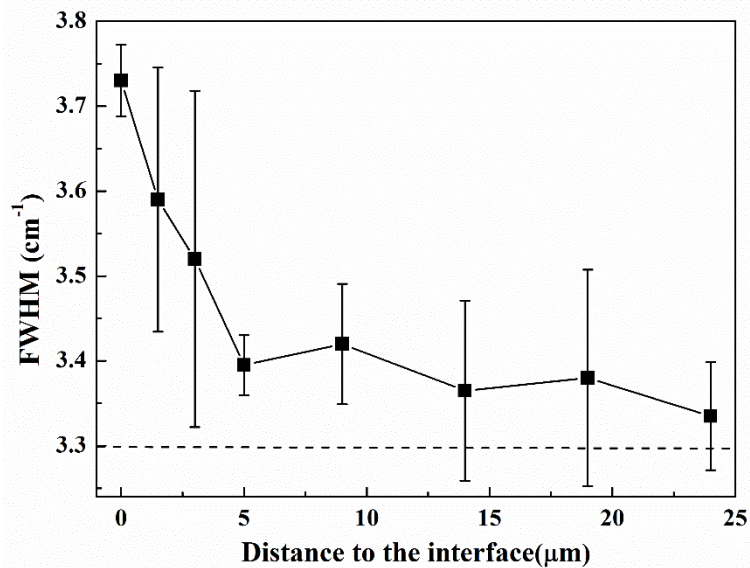
4. Strain measurement

The strain distribution in the region (scan 2 of the Fig. S2(a)) where the interface was vertical to the Y axis was also measured by both EBSD and CRM, and their results were shown in Fig. S4 and Fig. S5. Comparing the SEM image and each EBSD strain image, the irradiated/unirradiated interface is located at the position about 10 nm from the top edge. The statistical results of strain distribution for EBSD and CRM are shown in Fig. 3(b) and Fig. 3(d) of manuscript, respectively.
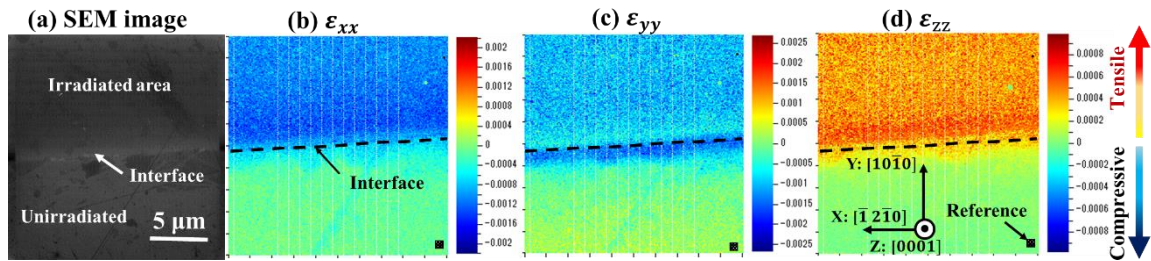

Fig. S4. Strain distribution around the irradiated/unirradiated interface. The interface is vertical to the Y axis under this EBSD scanning condition. (a) SEM image, (b–d) residual elastic strains (b) ε_{xx}, (c) ε_{yy}, and (d) ε_{zz}, respectively representing the strain horizontal (X), vertical (Y) and normal to the sample surface (Z). The EBSD pattern obtained from the black dot (Reference) is regarded as the reference for the strain analysis. These images correspond to the Fig. 3(b) of manuscript.
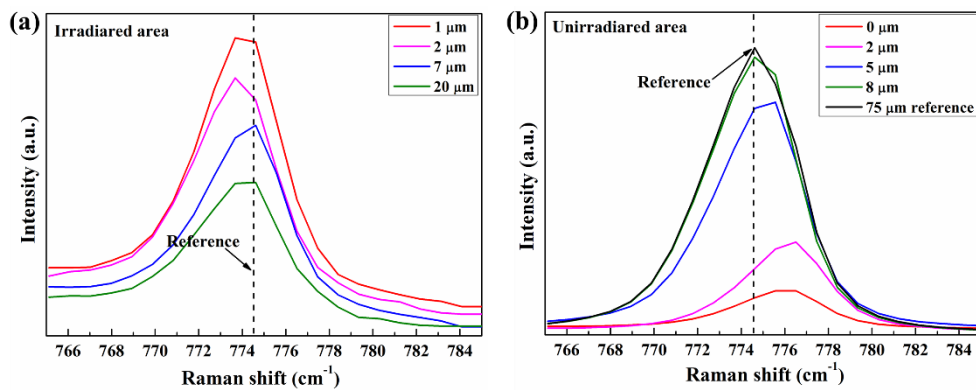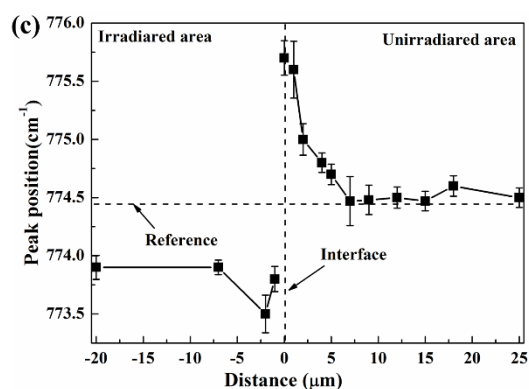
Fig. S5. Peak shift of $E_2(TO)$ in the (a) irradiated and (b) unirradiated areas. The insert numbers represent the distance from the interface. (c) Peak position of $E_2(TO)$ as a function of the distance to the interface. These results correspond to the Fig. 3(d) of manuscript.